Hierarchical Phosphorylation of HOXB13 by mTOR Dictates Its Activity and Oncogenic Function in Prostate Cancer

Yonghong Chen[1,2], Catherine R. Dufour[1], Lingwei Han[1,2], Ting Li[1], Hui Xia[1,2], and Vincent Giguère[1,2]

ABSTRACT

Dysregulation of mTOR signaling plays a critical role in promoting prostate cancer growth. HOXB13, a homeodomain transcription factor, is known to influence the androgen response and prostate cancer development. Recently, HOXB13 was found to complex with mTOR on chromatin. However, the functional crosstalk between HOXB13 and mTOR remains elusive. We now report that mTOR directly interacts with and hierarchically phosphorylates HOXB13 at threonine 8 and 41 then serine 31 to promote its interaction with the E3 ligase SKP2 while enhancing its oncogenic properties. Expression of HOXB13 harboring phosphomimetic mutations at the mTOR-targeted sites stimulates prostate cancer cellular growth both *in vitro* and in murine xenografts. Transcriptional profiling studies revealed a phospho-HOXB13–dependent gene signature capable of robustly discriminating between normal prostate tissues, primary and metastatic prostate cancer samples. This work uncovers a previously unanticipated molecular cascade by which mTOR directly phosphorylates HOXB13 to dictate a specific gene program with oncogenic implications in prostate cancer.

Implications: Control of HOXB13 transcriptional activity via its direct phosphorylation by the mTOR kinase is a potential therapeutic avenue for the management of advanced prostate cancer.

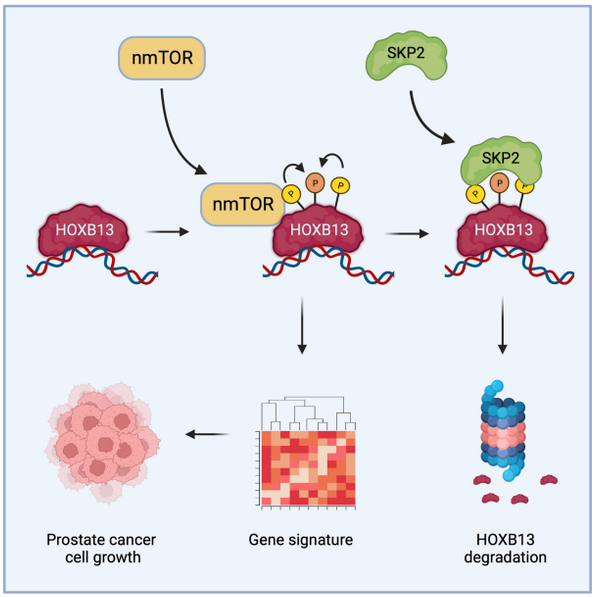

Introduction

Prostate cancer is one of the most diagnosed cancers in men worldwide. Androgen and its receptor (AR) play important roles in the progression of prostate cancer; hence, androgen deprivation therapy (ADT) is used as the standard treatment post-surgery or -radiation intervention. While many patients initially respond positively to ADT, the disease often develops into castration-resistant prostate cancer (CRPC; ref. 1), which is frequently metastatic with poor prognosis. Although AR remains hyperactive in CRPC, the emergence of drug resistance to AR inhibitors confers prostate cancer androgen-independent properties that lead to AR cistrome and transcriptome reprogramming by dysregulated cofactors (2). Therefore, in addition to AR-targeted therapies, alternative therapeutic targets are urgently needed (3), with AR cofactors being rational targets for exploration into their underlying regulatory mechanisms (4).

HOXB13, a homeobox family transcription factor essential for the development of a healthy prostate epithelium (5), is a well-known AR cofactor which confers cellular responses to androgen (6). It exerts dual roles in AR signaling by both activating and suppressing the transcription of AR target genes (7–9). Germline *HOXB13* (G84E) mutations have also been identified in a subset of familial prostate cancer (10). Paradoxically, HOXB13 has been shown to either promote or suppress prostate cancer cell growth and metastasis (11–14). These discrepancies may be attributed to the different experimental strategies that were used to assess the role of HOXB13 in prostate cancer cells (6). In addition, long-term versus short-term effects of HOXB13 modulation may also play a key role in determining its function in prostate cancer biology. While known mechanisms controlling HOXB13 activity are limited, recent studies have pointed towards posttranslational modifications (PTM). In particular, acetylation of HOXB13 at K277 by p300 increases its stability and confers tamoxifen resistance in breast cancer cells (15) and its dephosphorylation at S204 by calcineurin promotes its nuclear translocation and facilitates cardiomyocyte cell-cycle arrest (16). Little is known about regulation of HOXB13 activity by PTMs in the context of prostate cancer.

[1]Goodman Cancer Institute, McGill University, Montréal, Québec, Canada. [2]Department of Biochemistry, Faculty of Medicine and Health Sciences, McGill University, Montréal, Québec, Canada.

Corresponding Author: Vincent Giguère, Goodman Cancer Institute, McGill University, 1160 Pine Ave West, Montreal, QC, H3A 1A3, Canada. E-mail: vincent.giguere@mcgill.ca

Mol Cancer Res 2023;21:1050–63

doi: 10.1158/1541-7786.MCR-23-0086

mTOR, mammalian target of rapamycin, is a serine/threonine kinase belonging to the PI3K-related kinase family (17). It functions as the central catalytic subunit in two distinct protein complexes, mTORC1 and mTORC2. mTORC1 is defined by its unique component RAPTOR while RICTOR is specific to mTORC2 (18). Each complex usually phosphorylates a distinct set of substrates in different subcellular localizations, mainly in the cytoplasm, to regulate cell growth by promoting anabolic processes including protein, lipid, and nucleotide synthesis, and by suppressing catabolic processes like autophagy (19–21). In addition, emerging evidence highlights that mTOR and mTORC1/2 components can translocate into the nucleus and that nuclear mTOR can functionally interact with transcriptional regulators to coordinate gene transcription with cellular metabolism in a more direct manner (22, 23). Notably, we have previously shown that androgen signaling drives prostate cancer progression in part by promoting mTOR nuclear localization and its genomic reprogramming leading particularly to enhanced mTOR-AR interaction on DNA (24, 25). HOXB13 binding motif was found enriched at mTOR-bound loci, suggesting a functional genomic association between mTOR and HOXB13, a notion further corroborated by the identification of HOXB13 as an mTOR interactor in the recent characterization of the mTOR chromatin-bound interactome by rapid immunoprecipitation mass spectrometry (MS) of endogenous protein (RIME) in prostate cancer cells (26). Furthermore, canonical mTOR signaling has been shown previously to be activated by androgens, including the synthetic androgen R1881 (24, 27, 28).

In this study, we sought to further investigate the functional connection between nuclear mTOR and HOXB13. We show that mTOR directly interacts with and phosphorylates HOXB13 in the nucleus of prostate cancer cells. Phosphorylation of HOXB13 by mTOR at threonine 8 and 41 primes its further phosphorylation at serine 31, which triggers its E3 ligase SKP2 licensed proteasome-mediated degradation. Remarkably, although this mTOR-mediated phosphorylation cascade promotes HOXB13 destabilization, it augments HOXB13 oncogenic function. We provide evidence that expression of a HOXB13 phosphomimetic mutant of the three mTOR-targeted residues, but not the non-phosphorylatable mutant, promotes prostate cancer cellular growth *in vitro* and tumor growth *in vivo* in a xenograft model system. Furthermore, transcriptome analyses identified a phospho-HOXB13–targeted gene signature capable of discriminating normal prostate tissue, primary, and metastatic tumors in three human clinical cohorts. Taken together, our results reveal a previously unrecognized oncogenic regulatory circuit involving mTOR-mediated phosphorylation and destabilization of HOXB13, which could be envisaged as a therapeutic avenue in the management of prostate cancer.

Materials and Methods

Reagents

A complete list of reagents used in this study are presented in Supplementary Table S3.

DNA constructs and transfection

Short hairpin RNA (shRNA) targeting *TSC1*, *TSC2*, *RAPTOR*, *RICTOR*, and *SKP2* as well as pLX317 V5-tagged ORF of *Rheb*, *SKP2*, *HOXB13*, and GFP were provided by the Genetic Perturbation Service of the Goodman Cancer Institute at McGill University. Inducible shRNAs of mTOR and HOXB13 were self-cloned by inserting the short hairpin sequence into the inducible shRNA pLKO-TetON backbone (Addgene, catalog no. 21915). Inducible V5-tagged ORF of HOXB13 was made by inserting *HOXB13*-V5 sequence into a pCW57-Blasticidine inducible backbone (Addgene, catalog no. 80921). HOXB13 mutants (including shRNA2-resistant mutant, 3A, 3D, G84E and other point mutations) were mutated from WT *HOXB13*-V5 constructs by using a Q5 site-directed mutagenesis kit (NEB, catalog no. E0554S). GST-HOXB13 WT and mutants (T8A, T41A and T8A+T41A) were cloned into a pGEX-5X-3 backbone. DNA sequences encoding HOXB13 domain fragments (N-terminal and C-terminal) were cloned into a pLPC-3xFlag backbone, while mTOR domain fragments (N-terminal, Middle, and C-terminal) were generated by deletion strategy using a Q5 mutagenesis kit. HA-Ubiquitin (catalog no. 18712) and YFP-mTOR (catalog no. 73384) were purchased from Addgene. See also Supplementary Table S3 for further details.

Plasmid transfection

Calcium phosphate precipitation was used to transiently transfect 293T cells. Viral infections consisted of co-transfection of lentivirus packaging vector psPAX2 (Addgene, catalog no. 12260) and envelop vector pMD2.G (Addgene, catalog no. 12259) with shRNAs or ORFs of target genes into 293T cells to first generate lentivirus. LNCaP and PC3 cells were infected by the virus supplemented with 8 μg/mL polybrene and selected by 1 μg/mL puromycin or blasticidine.

Stable LNCaP cells

LNCaP cells were infected with lentivirus containing HOXB13 inducible shRNA to knockdown endogenous HOXB13. Lentivirus containing inducible HOXB13 mutants were used to infect LNCaP-shHOXB13 stable cells for rescuing expression. For experiments, 1 μg/mL doxycycline was added to these stable LNCaP cells to induce the expression of HOXB13 shRNA and HOXB13 mutants simultaneously whereby endogenous HOXB13 is knocked down and rescued with exogenous HOXB13 mutants.

Cell culture

LNCaP (RRID:CVCL_0395), PC3 (RRID:CVCL_0035), 22RV1 RRID:CVCL_1045), HEK293T (RRID:CVCL_0063), and Hela (RRID:CVCL_0030) cell lines were specifically purchased from the ATCC for this study and reauthenticated using markers specific for each cell line as previously described (26). Prostate cancer cell lines were cultured in phenol-red free RPMI medium (Wisent, catalog no. 350–046CL) supplemented with 10% FBS (Thermo Fisher Scientific, catalog no. 12483020). HEK293T and Hela cell lines were maintained in DMEM medium (Wisent, catalog no. 319–005CL) supplemented with 10% FBS. *Mycoplasma* was regularly monitored using a Mycoplasma PCR Detection Kit (Applied Biological Materials, catalog no. G238) and no contamination was detected (latest test performed in December 2022). Cells were not kept in culture for more than 25 passages. For treatment with R1881 (Steraloids, catalog no. E3164–000), LNCaP cells were plated and grown in 150 mm culture dishes to ∼75% confluency before switching to medium containing 2% CSS medium for 48 hours to deprive cells of steroids prior to treatment with 10 nmol/L R1881 in freshly added CSS medium for another 24 hours or as indicated.

Immunoblotting

For cultured cells, cell culture medium was discarded and washed once with ice-cold 1 X PBS prior to protein lysate preparation. For cytosolic/nuclear fractionation, 1 mL Harvest Buffer (10 mmol/L Hepes, 50 mmol/L NaCl, 0.5 mol/L Sucrose, 10 mmol/L EDTA, 0.5% Triton X-100 and protease inhibitors) was added per 150-mm

plate for cell lysis. Cells were scraped, and lysates were incubated on ice for 8 minutes before being centrifuged at 3,000 rpm, 4°C for another 8 minutes. The supernatants were collected and centrifuged further at 12,000 rpm, 4°C for 15 minutes. The resulting supernatants were kept as the cytosolic fractions and the nuclear pellets were washed twice with Buffer A (10 mmol/L Hepes, 10 mmol/L KCl, 0.1 mmol/L EDTA, and 0.1 mmol/L EGTA). Nuclear pellets were re-suspended in Buffer K (20 mmol/L phosphate buffer PH7.4, 150 mmol/L NaCl, 0.1% NP40, 5 mmol/L EDTA and protease inhibitors) supplemented with 0.6% CHAPS and rotated at 4°C for at least 40 minutes. Brief sonication was used to ensure efficient extractions. The nuclear lysates were collected after centrifugation at 12,000 rpm, 4°C for 15 minutes. For whole cell lysates, cells were directly lysed in Buffer K supplemented with 0.6% CHAPS for at least 40 minutes on ice. The supernatants were collected after being centrifuged at 12,000 rpm, 4°C for 15 minutes.

For xenograft tumor lysates, frozen tumors were pulverized in liquid nitrogen and ∼50 to 100 μL frozen tumor powder were resuspended in ∼500 to 1,000 μL Buffer K and sonicated at $P = 3$ for 20 seconds and repeated once. Samples were then rotated at 4°C for 40 minutes for efficient protein lysis. The supernatants were collected after centrifugation at 12,000 rpm, 4°C for 15 minutes.

For IP, at least 5 confluent 150-mm plates (per treatment condition) of LNCaP or 22rv1 cells were extracted in Buffer K supplemented with 0.6% CHAPS for nuclear IPs. For each nuclear IP, 2 μg antibody was pre-incubated with 1 mg Protein G magnetic beads (Invitrogen, catalog no. 10009D) at room temperature for 1 hour, then ∼0.3 to 1 mg nuclear protein was added to the antibody-beads mixture and left to rotate at 4°C overnight. The next day, the beads were washed 3 times with 1x PBST containing 0.1% Tween and heated to 70°C for 5 minutes in 1x Western Loading Buffer.

Protein concentration was measured using Bradford reagent (Bio-Rad, catalog no. 500–0006). Generally, 20 to 30 μg of proteins was mixed with 1x Western Loading Buffer and heated at 95°C for 5 minutes before being loaded on 6% to 9% SDS-PAGE gels for immunoblotting as previously described (26). Primary and secondary antibodies are listed in Supplementary Table S3. Uncropped blots (indicated by red boxes) used to generate the figures are shown in Supplementary Fig. S6.

Lambda phosphatase treatment

293T cells were transiently transfected with vectors expressing HOXB13 mutants (WT, T8D, T41D or T8D+T41D). After extracting whole cell lysates, V5-tag immunoprecipitation was performed to pull down the exogenous HOXB13 mutants followed by addition of lambda phosphatase to digest the immunoprecipitates directly in the tubes for 30 minutes.

mTOR *in vitro* kinase assay

GST-HOXB13 WT (pGEX-5x-3 backbone) and mutants were transformed into BL21 bacteria, and their expression was induced by 0.4 mmol/L IPTG for 4 hours at 30°C after reaching a 0.6 O.D. (600 nm) absorbance at 37°C. Bacteria were collected and lysed in STE buffer (10 mmol/L Tris-HCl pH 8.0, 1 mmol/L EDTA, 100 mmol/L NaCl, 5 mmol/L DTT, and protease inhibitors) with 1 mg/mL lysozyme (Roche, catalog no. 10837059001) and 1.5% Sarcosyl (Sigma, catalog no. L5125) for 30 to 45 minutes prior to sonication.

Glutathione Sepharose beads (GE HealthCare, catalog no. 17–0756–01) were washed twice with NETN buffer (10 mmol/L Tris-HCl pH 8.0, 1 mmol/L EDTA, 100 mmol/L NaCl, 0.5% NP-40) and rotated together with bacterial lysate containing GST-HOXB13 protein at 4°C for 2 hours. Beads were then washed twice with NETN buffer, twice with high salt NETN buffer (10 mmol/L Tris-HCl pH 8.0, 1 mmol/L EDTA, 500 mmol/L NaCl, 0.5% NP-40), and once more with NETN buffer. After washing, GST-HOXB13 protein was eluted from the beads by adding freshly prepared pH 8.8 Elution Buffer (25 mmol/L glutathione, 50 mmol/L Tris pH 8.8, 200 mmol/L NaCl) and rotating at 4°C for 30 minutes. After brief centrifugation, the supernatant containing pure GST-HOXB13 protein was collected as the substrate for an mTOR kinase assay described below.

mTOR was IP'd from Hela cells (with or without 300 nmol/L insulin stimulation for 30 minutes) lysed in mTOR lysis buffer (40 mmol/L HEPES pH 7.4, 2 mmol/L EDTA, 10 mmol/L Pyrophosphate, 10 mmol/L Glycerophosphate, 0.3% CHAPS). Briefly, magnetic Protein G beads (Invitrogen, catalog no. 10009D) bound with target proteins were washed 3 times with low salt wash buffer (40 mmol/L HEPES PH 7.4, 2 mmol/L EDTA, 10 mmol/L Pyrophosphate, 10 mmol/L Glycerophosphate, 0.3% CHAPS, and 150 mmol/L NaCl) and twice with equilibrium buffer (25 mmol/L HEPES pH 7.4, 20 mmol/L KCl). The mTOR kinase assay was then performed by mixing Protein G beads containing mTOR kinase, 0.5 μg GST-HOXB13 protein purified from bacteria, 50 μmol/L unlabeled ATP and 5 μCi P^{32}-ATP together in mTOR kinase buffer (25 mmol/L HEPES PH 7.4, 50 mmol/L KCl, 10 mmol/L MgCl2, 4 mmol/L MnCl2, 1 mmol/L DTT, 20% Glycerol) at 30°C for 40 minutes. The reaction was stopped by the addition of Western loading buffer and the mixture was boiled at 95°C for 5 minutes. Heat-denatured samples were separated on a 12% SDS-PAGE gel. The radioactive gel was dried, exposed to Fuji Storage Phosphor Screen, and viewed by the Typhoon TRIO Variable Mode Imager (Amersham Biosciences). The gel was also stained with Coomassie brilliant blue to confirm that an equal amount of GST-HOXB13 protein substrate was used in each reaction.

GST pull-down

During protein extraction and purification from bacteria, GST-tagged HOXB13 protein or the GST tag only were bound with Glutathione Sepharose Beads (GE HealthCare, catalog no. 17–0756–01) which served as the bait. For the prey proteins, we used 293T whole cell lysates which were precleared with unbound Glutathione Sepharose Beads. Precleared supernatant (prey) was directly added to and mixed with GST-HOXB13 or GST-bound Glutathione Sepharose Beads (bait). Binding buffer (1xPBS+ 0.1% Tween 20, 0.25 mmol/L DTT) was added to a final volume of 1 mL and the mixture was rotated at 4°C overnight. The next day, the beads were washed 3 times with binding buffer by pipetting up and down. Western loading buffer was added, and the beads were boiled at 95°C for 5 minutes before loading on the gel.

MS (in gel digestion)

Following the mTOR *in vitro* kinase assay (with only unlabeled ATP) using GST-HOXB13 as the substrate, denatured proteins were separated by SDS-PAGE. Coomassie Brilliant Blue R250 was used for gel staining to visualize the protein bands. A piece corresponding to the size of GST-HOXB13 was cut and sent for MS analysis. Chymotrypsin was used for digestion. Phosphopeptides detected with > 80% probably were considered high-confident phosphosites.

RT-qPCR

Total RNA from cells or frozen xenograft tumor powder (∼30 μL) was extracted using a RNeasy Mini Kit (Qiagen, catalog no. 74106). RNA (1 μg) was reverse transcribed using ProtoScript II Reverse Transcriptase (NEB, catalog no. M0368X) and measured by quantitative real-time PCR using SYBR Green Master Mix (Roche, catalog

no. 4887352001) on a LightCycler 480 instrument (Roche). The relative expression levels of target genes were normalized to the average expression of two human housekeeping genes (*TBP* and *ACTB*). For RNA sequencing (RNA-seq) samples, a DNase I (Qiagen, catalog no. 79254) digestion step was additionally performed during RNA extraction to eliminate DNA contamination. Specific human RT-qPCR primer sequences are listed in Supplementary Table S3.

RNA-seq and analysis

Messenger RNA-seq profiling was performed by Novogene Bioinformatics Technology Co., Ltd. Sample libraries prepared using the NEBNext Ultra II RNA Library Prep kit were sequenced on an Illumina platform (NovaSeq 6000) and 150 bp paired-end reads were generated. Raw data of fastq format were processed through in-house perl scripts to remove reads containing adapter and poly-N sequences and reads with low quality. Hisat2 software (version 2.0.5) was used to align paired-end clean reads to the Homo Sapiens reference genome hg38 and Feature Counts software (version 1.5.0-p3) was used to count the number of reads mapped per gene. FPKM (Fragments per kilobase of transcript sequence per millions base pairs sequenced) of each gene was calculated on the basis of the length of the gene and read counts mapped to this gene. Differential expression analysis between the groups was performed using the DESeq2 R package (version 1.20.0). Significant differentially expressed genes (DEG) between groups ($n = 3$ per group) were determined using DESeq2 P value < 0.05 and an absolute $\log_2$ fold-change > 0.5. In addition, probes with an attributed value of zero in expression found in at least 1 sample among the comparative groups were filtered out. HOXB13- and mTOR-dependent DEGs ± vehicle (EtOH) or R1881 for 24 hours are presented in Supplementary Tables S1 and S2, respectively. Total DEGs found dependent on phospho-HOXB13 (354 genes) ± R1881 are presented in Supplementary Table S1. Total DEGs found dependent on mTOR (3812 genes) or common to phospho-HOXB13 and mTOR (106) ± R1881 are presented in Supplementary Table S2. Note that Heat maps of DEGs using z-scaled $\log_2$(FPKM+1) values were generated using Morpheus (https://software.broadinstitute.org/morpheus/). Functional enrichment analysis of DEGs was performed using Enrichr (29) (https://maayanlab.cloud/Enrichr/) to identify enriched Molecular Signature Database (MSigDB) hallmark signatures (v 2020). For clustering analyses, microarray data from public human clinical datasets were first filtered to include probes associated with phospho-HOXB13–dependent genes. In Gene Cluster 3.0 (30), probes with expression values present across 80% of the samples and a MaxVal–MinVal cutoff > 1.0 were retained and hierarchical clustering using average linkage and the distance metric correlation (uncentered) was performed on log transformed data with genes centered on means. Clustering results were visualized using Java TreeView 3.0 (v beta 1; https://doi.org/10.5281/zenodo.1303402). Interrogated datasets were GSE6099 (31), GSE3325 (32), and GSE8511. The 354-geneset regulated by phospho-HOXB13 was first assessed on the Tomlins and colleagues (31) cohort and the resulting validated list of 127 mapped genes (listed in Supplementary Table S1) were used to further interrogate the cohorts in GSE3325 and GSE8511.

Colony formation assay

6,000 LNCaP cells were seeded evenly per well in 6-well plates. After ~3 weeks (changing the medium every 5 days) cell colonies grew out. Cells were washed once with cold 1 X PBS and 100% methanol was added for 20 minutes at room temperature to fix the colonies in the plates. Three washes with cold 1 X PBS were done to remove the methanol before adding Crystal Violet (Sigma, catalog no. V5265) for 10 minutes at room temperature to stain the colonies. Cold 1 X PBS was used to wash out the unbound Crystal Violet at least 3 times to get achieve a clear background. The plates were air dried at room temperature and pictures were taken.

Incucyte cell proliferation assay

A total of 3,000 LNCaP cells were seeded evenly per well in 96-well plates. Six replicates were prepared for each experimental condition. Cell plates were incubated in an Incucyte incubator where cellular growth was monitored over 1 week, and cell confluency was quantified. One-way ANOVA test was used to calculate the statistical significance.

Xenograft tumor growth

Mouse manipulations were performed as approved by the McGill Facility Animal Care Committee and complied with ethical guidelines set by the Canadian Council of Animal Care. NSG mice (14-weeks old) were used for the LNCaP tumor xenografts. Three million cells were mixed with Matrigel (VWR, catalog no. 354262; v/v is 2/1, 100 μL in total per mouse) and subcutaneously injected into the right side of each mouse. Six mice were injected for each of the 5 established LNCaP cell lines. Doxycycline (Wisent Bioproducts, catalog no. 450–185) was administered in the drinking water at 2 mg/mL (Dox water) and given to mice following injection to induce gene expression. Every 6 days, the Dox water was freshly replaced considering the instability of doxycycline at room temperature. Around 16 days after the cell injections, the first tumor was observed, after which tumors were monitored and volumes were measured every 3 days. Tumor volume was determined by caliper measurements of two dimensions and calculated using the formula $V = L^*W^*W/2$ where V = volume, L = length, and W = width. When the largest tumor reached the maximal permitted size (2 cm^3), all mice were sacrificed at the same time. Tumors were collected, weighed, snap-frozen in liquid nitrogen and stored at −80°C.

Statistics

GraphPad Prism 9 software was used to draw graphs and for statistical analyses. The number of independent experiments or biological replicates used are indicated in the figure legends. Unless otherwise specified, differences were considered significant when P value calculated by one-way ANOVA analysis was less than 0.05.

Data availability

All RNA-seq datasets have been deposited in NCBI's Gene Expression Omnibus (GEO) and are accessible through GEO SuperSeries accession number GSE225207 encompassing SubSeries GSE225206 (HOXB13 RNA-seq) and GSE225205 (mTOR RNA-seq). Public human clinical microarray data used in this study are available from the GEO database: GSE6099 (31), GSE3325 (32), and GSE8511. Source data underlying the graphs are presented in Supplementary Table S4. Uncropped immunoblots are shown in Supplementary Fig. S6.

Results

mTOR regulates HOXB13 protein stability

To explore a possible role for mTOR in regulating the activity of HOXB13, we first tested whether perturbing mTOR function could influence the expression of HOXB13 in prostate cancer cells. Three HOXB13 positive human prostate cancer cell lines were used to monitor the effect of mTOR inhibitors, Torin1 and rapamycin, on HOXB13 expression: LNCaP ($AR^+/PTEN^-$), 22Rv1 (AR and AR variant$^+$/$PTEN^+$) and PC3 ($AR^-/PTEN^-$). Treatment with either

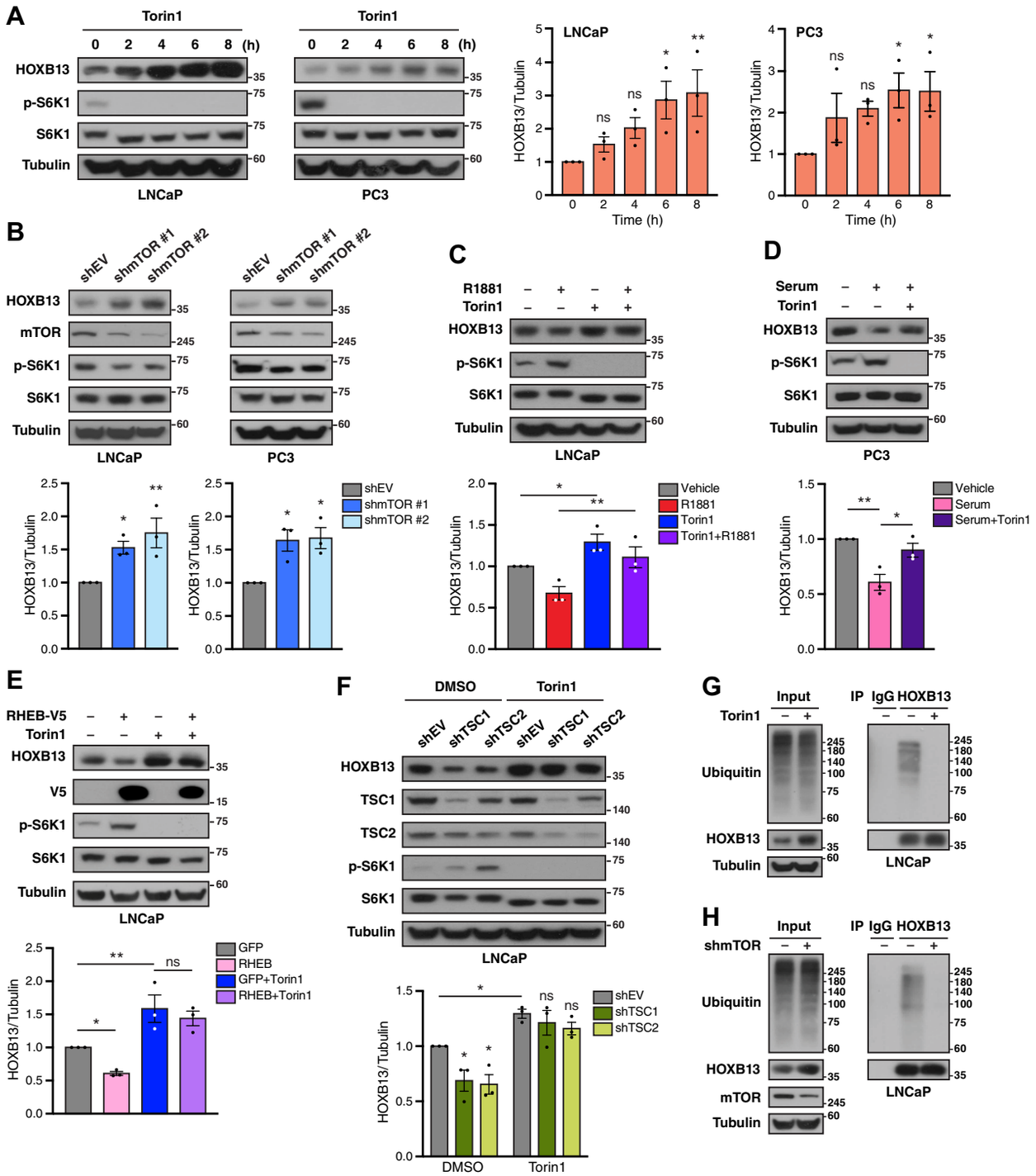

Figure 1.
mTOR negatively regulates HOXB13 protein stability. **A,** Time course treatment of LNCaP and PC3 cells with the mTOR inhibitor Torin1 (100 nmol/L). **B,** Detection of HOXB13 protein levels in LNCaP and PC3 cells with mTOR knockdown using two inducible shRNAs (induced by 1 μg/mL Doxycycline for 3 days). **C,** Assessment of HOXB13 protein levels in LNCaP cells that were androgen deprived for 48 hours prior to treatment with the synthetic androgen R1881 (10 nmol/L) and/or Torin1 (100 nmol/L) for another 24 hours. **D,** PC3 cells were serum-starved for 24 hours and then stimulated by 10% serum ± 100 nmol/L Torin1 for another 24 hours. **E,** HOXB13 immunoblot analysis in LNCaP cells with genetic overexpression of the mTOR upstream activator RHEB ± pharmacologic inhibition of mTOR with Torin1 (250 nmol/L, 8 hours). **F,** HOXB13 immunoblot analysis in LNCaP cells with genetic knockdown of mTOR upstream inhibitor TSC1 or TSC2 ± pharmacologic inhibition of mTOR with Torin1 (250 nmol/L, 8 hours). **G,** HOXB13 polyubiquitination was examined in response to the mTOR inhibitor Torin1 (100 nmol/L) for 24 hours in LNCaP cells. **H,** HOXB13 polyubiquitination following inducible shRNA-mediated mTOR knockdown (1 μg/mL Dox, 3 days) in LNCaP cells. Relative HOXB13 protein levels were quantified and normalized over Tubulin using Image J software. Data in **A–F** represent means ± SEM of three independent experiments. Statistics were calculated by one-way ANOVA. *, $P < 0.05$; **, $P < 0.01$; ns, not significant.

Torin1 or rapamycin for 24 hours led to increased HOXB13 expression in LNCaP and PC3 cells (Supplementary Fig. S1A), two cell lines retained for further study. The increase in HOXB13 expression was rapid, augmenting as early as 2 hours following treatment with Torin1 with maximal levels attained by 8 hours (**Fig. 1A**). Efficacy of the drug-induced inhibition of mTOR was confirmed by decreased phosphorylation of S6K1 (**Fig. 1A**; Supplementary Fig. S1A). Consistent with pharmacologic inhibition of mTOR, genetic knockdown of mTOR using two distinct shRNAs also increased HOXB13 protein levels in both LNCaP and PC3 cells (**Fig. 1B**). Activation of canonical mTOR signaling by the synthetic androgen R1881 decreased HOXB13 levels, an effect lost by co-treatment with Torin1 (**Fig. 1C**). Torin1 had no significant impact on the expression of *HOXB13* mRNA levels, indicating that its regulation of HOXB13 expression is posttranscriptional (Supplementary Fig. S1B). In a similar fashion, serum stimulation of mTOR activity in PC3 cells decreased HOXB13 protein levels which were rescued by addition of Torin1 (**Fig. 1D**). In addition, stimulation of mTOR signaling by either overexpression of Rheb or knockdown of *TSC1/2*, two important but opposite regulators of mTOR activity, led to a reduction in HOXB13 levels in both LNCaP and PC3 cells (**Fig. 1E** and **F**; Supplementary Fig. S1C–S1E). This reduction in HOXB13 expression was dependent on mTOR kinase activity since co-treatment with Torin1 abolished the observed effects (**Fig 1**E and **F**; Supplementary Fig. S1C and S1E). Furthermore, shRNA-mediated genetic disruption of specific mTORC1 and mTORC2 component, RAPTOR and RICTOR, respectively, provoked an increase in HOXB13 levels in both LNCaP and PC3 cells (Supplementary Fig. S1F and S1G). These results suggest that both canonical mTOR complexes are involved in HOXB13 regulation. We next investigated whether the regulation of HOXB13 expression by mTOR involves changes in poly-ubiquitination of HOXB13. As shown in LNCaP and PC3 cells (**Fig. 1G** and **H**; Supplementary Fig. S1H and S1I), both pharmacologic inhibition (Torin1) and genetic disruption of mTOR (shRNAs) led to a sharp reduction in HOXB13 poly-ubiquitination, indicating less targeting of HOXB13 to the proteasome and thus its protection from degradation.

mTOR physically interacts with HOXB13

The presence of HOXB13 recognition motifs within mTOR chromatin-bound regions (24) together with the identification of HOXB13 and mTOR as partners from two recent proteomics

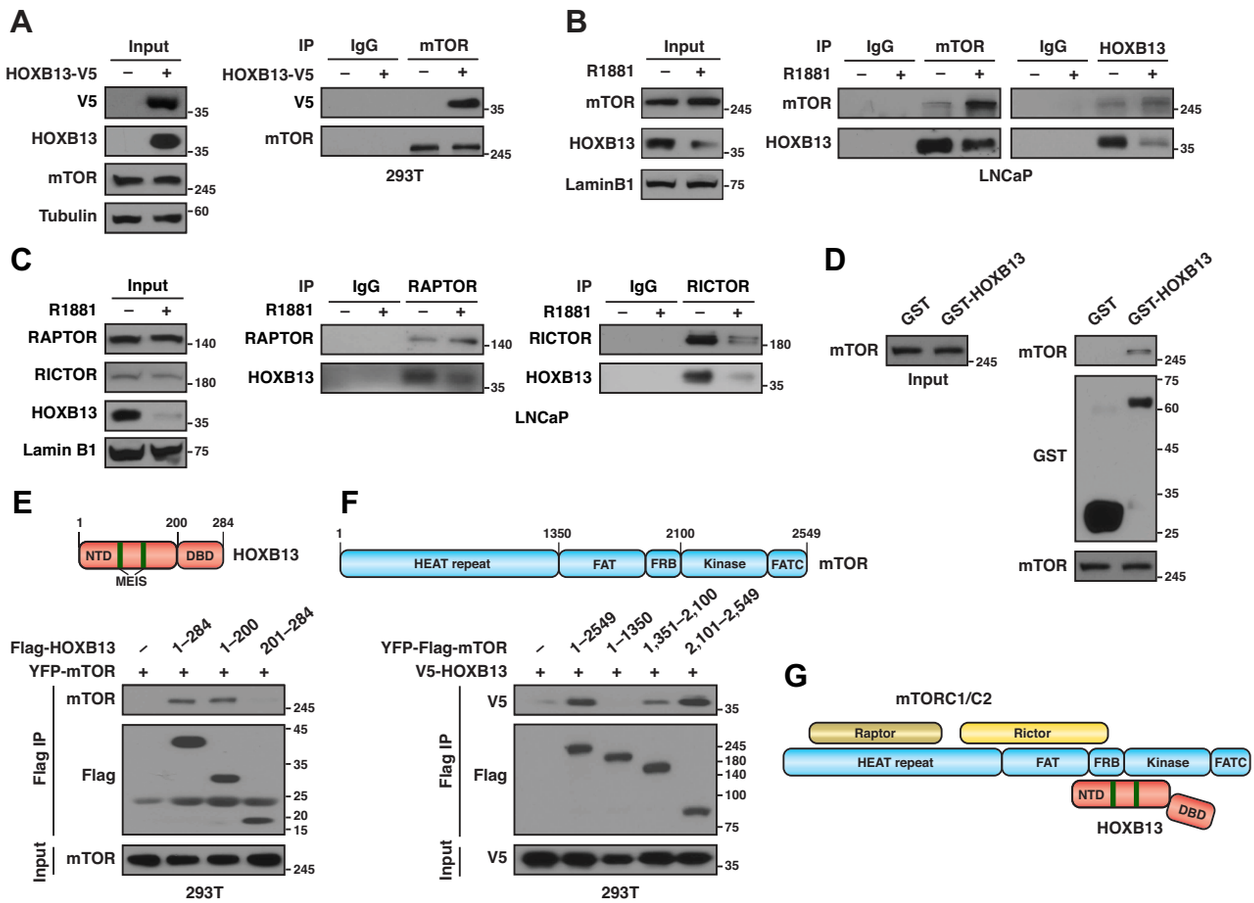

Figure 2.

mTOR physically interacts with HOXB13. **A,** mTOR co-IP with exogenously expressed HOXB13 in 293T cells. **B,** Co-IPs showing endogenous interaction between mTOR and HOXB13 in LNCaP cells ± R1881 (10 nmol/L, 48 hours). **C,** Specific mTORC1 (RAPTOR) and mTORC2 (RICTOR) components interact with HOXB13 in LNCaP cells ± R1881 (10 nmol/L, 48 hours) by co-IP. **D,** GST-HOXB13 protein purified from bacteria BL21 was used to pull-down mTOR from 293T whole cell lysates. **E,** HOXB13 N-terminal domain (NTD) interacts with mTOR in 293T cells. **F,** mTOR C-terminal kinase domain interacts with HOXB13 in 293T cells. HOXB13 also interacted with mTOR Middle domain but to a lesser extent. **G,** Schematic illustrating mTOR and HOXB13 interacting domains.

studies probing the mTOR and HOXB13 interactomes, respectively (26, 33), support the notion that mTOR and HOXB13 are components of the same complex(es). To explore mTOR and HOXB13 association further, we first performed co-immunoprecipitation (co-IP) assays in 293T cells expressing V5-tagged HOXB13. As shown (**Fig. 2A**), V5-tagged HOXB13 strongly complexes with endogenous mTOR. The formation of this complex can also be observed by co-IPs of endogenous proteins in LNCaP cells (**Fig. 2B**). In addition, both endogenous RAPTOR and RICTOR can also interact with HOXB13 in LNCaP cells (**Fig. 2C**). Significantly, *in vitro* GST pulldown assay established that the interaction between HOXB13 and mTOR is direct (**Fig. 2D**). To further map the functional domains involved in this interaction, we performed co-IP experiments in 293T cells co-expressing HOXB13 and mTOR full-length or truncation mutants. Our findings revealed that the amino-terminal domain of HOXB13 is required to complex with mTOR and reciprocally, the carboxy-terminal domain of mTOR, which includes the kinase domain, is necessary to complex with HOXB13 (**Fig. 2**E–**G**).

mTOR phosphorylates HOXB13

We next examined whether mTOR can phosphorylate HOXB13. *In vitro* kinase assay confirmed that HOXB13 is indeed a substrate of the mTOR kinase, with a higher degree of phosphorylation observed

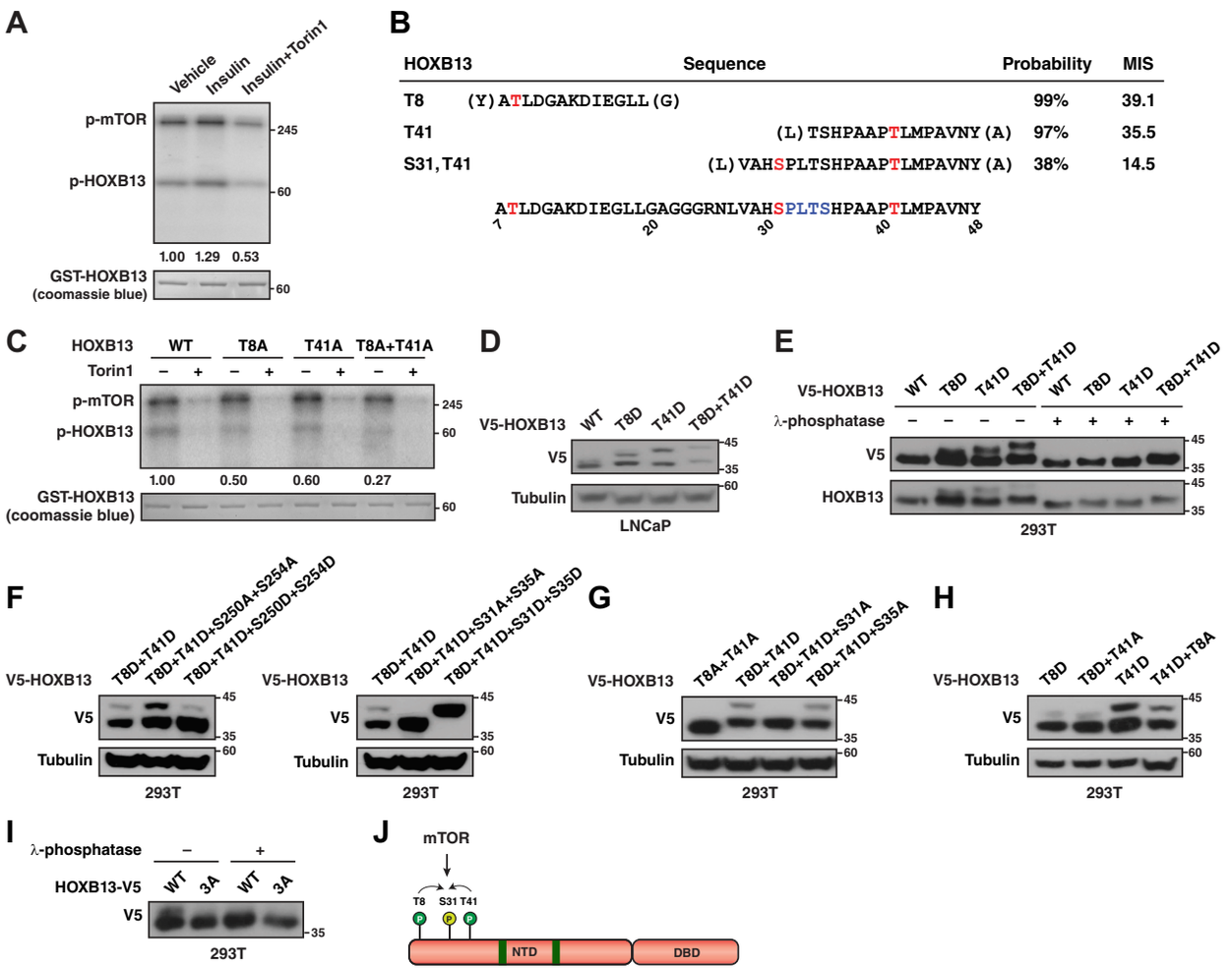

Figure 3.

mTOR directly phosphorylates HOXB13. **A,** mTOR *in vitro* kinase assay with GST-HOXB13 as the substrate. mTOR purified from Hela cells treated with insulin showed higher kinase activity, an effect abolished by co-treatment with the mTOR inhibitor Torin1. **B,** MS analysis of phosphorylated HOXB13 in (**A**) identified two HOXB13 phosphorylation sites (T8 and T41) with high probability. MIS, Mascot ion score. **C,** Alanine mutation of HOXB13 on T8 and T41 disabled its mTOR-mediated phosphorylation *in vitro*. **D,** HOXB13 phosphorylation mimics T8D, T41D, and T8D+T41D (plasmid) were transfected and stably expressed in LNCaP cells. Whole cell lysates were extracted for immunoblotting and one additional upper band was observed. **E,** HOXB13 phosphorylation mimics T8D, T41D, and T8D+T41D (plasmid) were transfected and transiently expressed in 293T cells. After extracting the whole cell lysates, V5 tag immunoprecipitation was used to pull down these HOXB13 mutants and Lambda phosphatase was used to digest the immunoprecipitates directly in the tubes for 30 minutes. Immunoblots showed that the upper band completely disappeared after brief phosphatase treatment, implicating the upper band was another phosphorylation band triggered by T8 or T41 phosphorylation. **F,** Serine (S) residues at sites 250/254 or sites 31/35 were mutated to Alanine (A) or Aspartic Acid (D) in HOXB13 T8D+T41D phosphomimic mutant. **G,** Single Alanine mutation was introduced to Serine 31 or 35 of HOXB13 T8D+T41D phosphomimic mutant. **H,** Alanine mutation of T41 and T8 was introduced to HOXB13 phosphomimic T8D and T41D, respectively. **I,** Immunoblot showing one additional band from V5-tagged HOXB13 immunoprecipitates of WT but not the 3A phospho-deficient mutant. Lambda phosphatase was used to confirm the upper band was a phosphorylation band. **J,** Schematic of HOXB13 phosphorylation primed by mTOR.

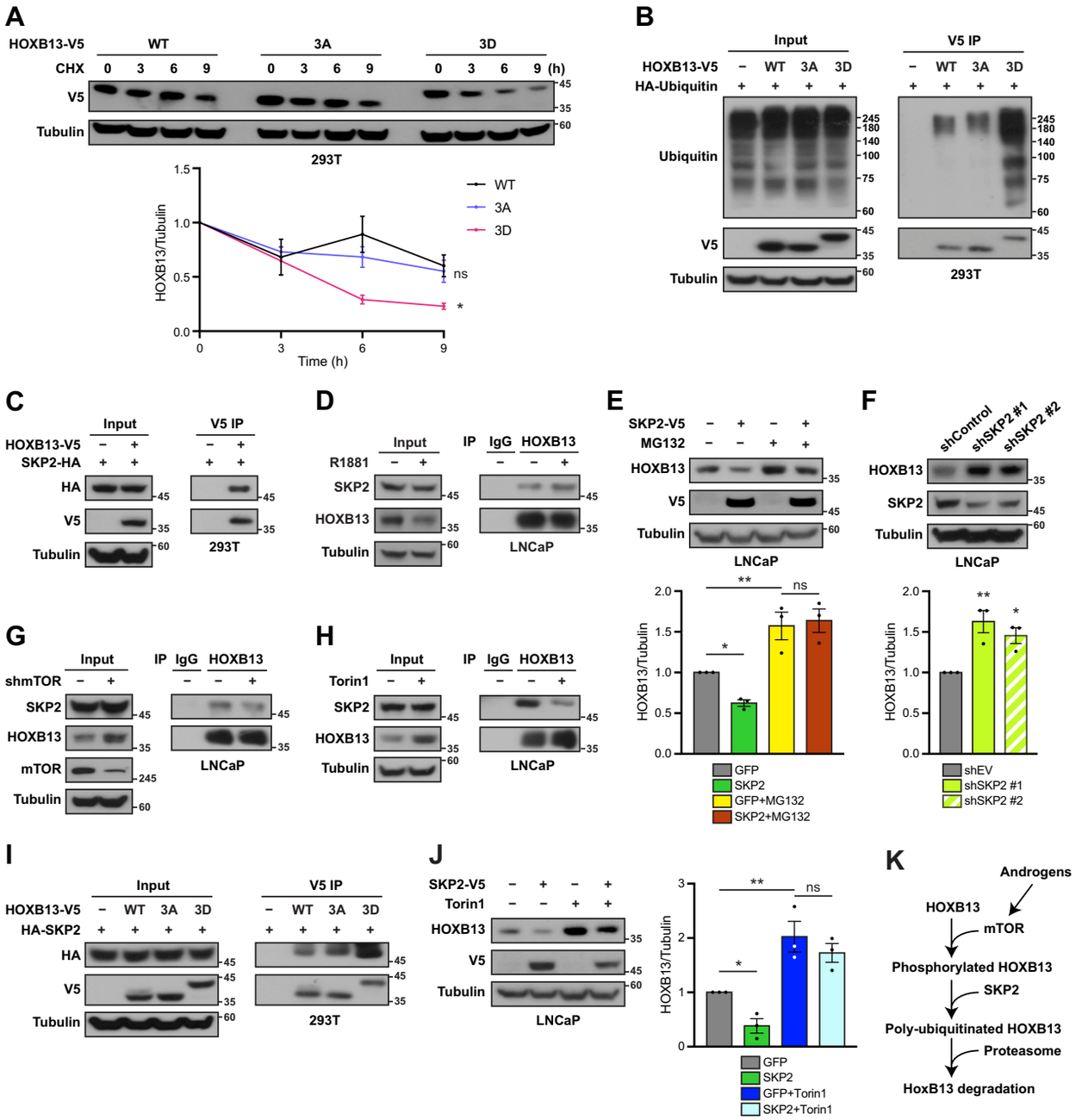

Figure 4.

HOXB13 phosphorylation promotes its degradation by SKP2. **A,** Protein synthesis inhibitor Cycloheximide was used to evaluate the protein stability of HOXB13 WT, phospho-deficient mutant (3A) and phospho-mimicking mutant (3D) expressed in 293T cells. **B,** Polyubiquitination of HOXB13 mutants were examined using 293T whole cell lysates. **C,** Exogenous HOXB13 interacted with E3 ligase SKP2 in 293T cells. **D,** HOXB13 and E3 ligase SKP2 interact endogenously in LNCaP cells ± R1881 (10 nmol/L, 24 hours). **E,** SKP2 overexpression decreased HOXB13 protein levels which were rescued by proteasome inhibitor MG132 (20 μmol/L, 8 hours) in LNCaP cells. **F,** Genetic knockdown of SKP2 increased HOXB13 protein levels in LNCaP cells. **G,** Inducible shRNA-mediated knockdown of mTOR (1 μg/mL Dox, 3 days) decreased HOXB13 interaction with SKP2 in LNCaP cells. **H,** Pharmacologic inhibition of mTOR (100 nmol/L Torin1, 24 hours) impaired HOXB13 interaction with SKP2 in LNCaP cells. **I,** HOXB13 phosphomimic mutant 3D interacted more strongly with SKP2 in 293T cells compared with WT or phospho-deficient mutant 3A. **J,** Diminished HOXB13 protein levels provoked by SKP2 overexpression was rescued by Torin1 treatment (250 nmol/L, 8 hours) in LNCaP cells. **K,** Schematic of mTOR primed and SKP2 licensed HOXB13 degradation. Relative HOXB13 protein levels were quantified and normalized over Tubulin using Image J software. Data in **A, E, F,** and **J** represent means ± SEM of three independent experiments. Statistics were calculated by one-way ANOVA. *, $P < 0.05$; **, $P < 0.01$; ns, not significant.

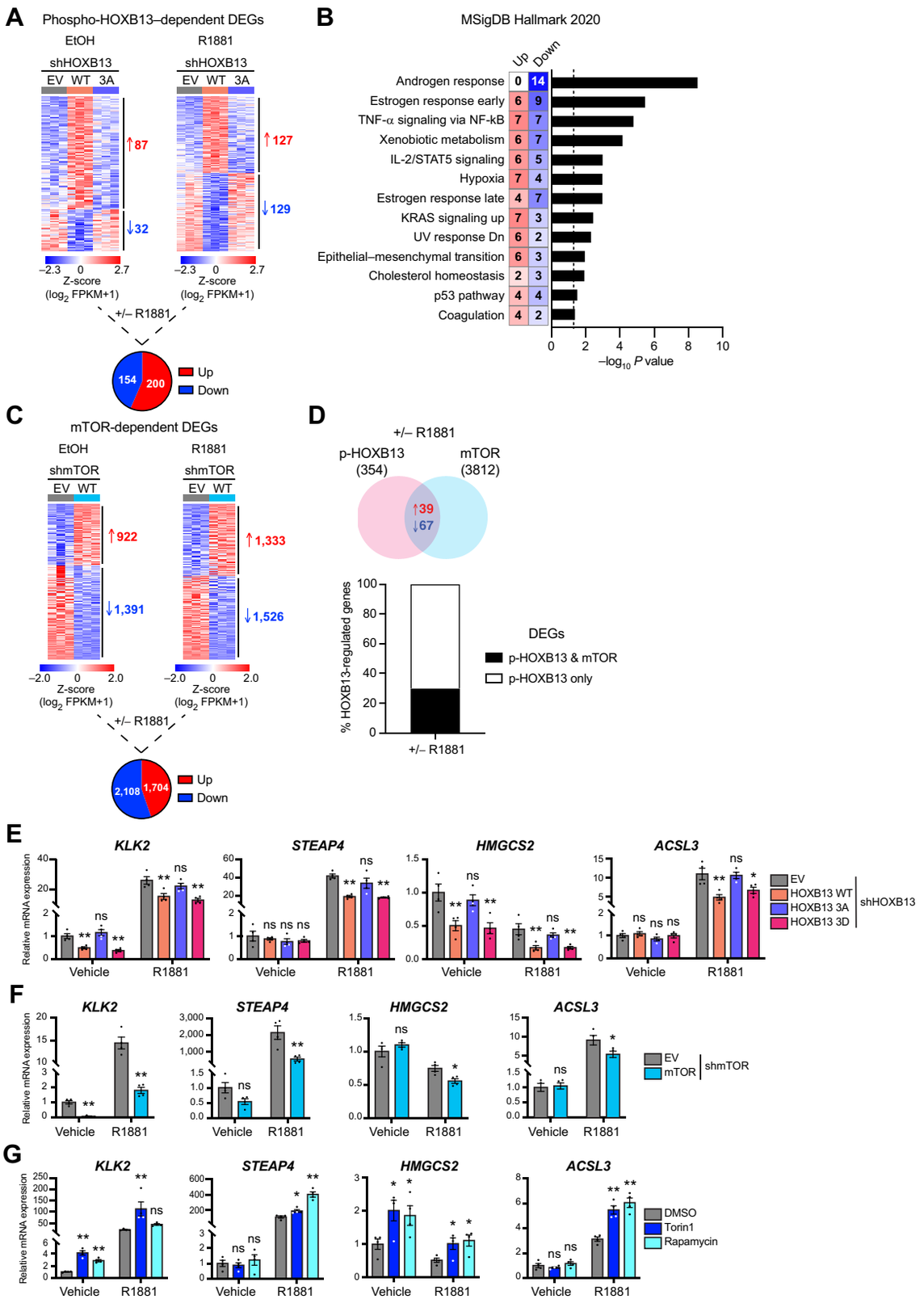
A
Phospho-HOXB13–dependent DEGs
EtOH
R1881
shHOXB13
EV WT 3A
↑87
↓32
↑127
↓129
−2.3 0 2.7
Z-score
(log2 FPKM+1)
+/− R1881
154
200
Up
Down
B
MSigDB Hallmark 2020
Up Down
Androgen response 0 14
Estrogen response early 6 9
TNF-α signaling via NF-kB 7 7
Xenobiotic metabolism 6 7
IL-2/STAT5 signaling 6 5
Hypoxia 7 4
Estrogen response late 4 7
KRAS signaling up 7 3
UV response Dn 6 2
Epithelial–mesenchymal transition 6 3
Cholesterol homeostasis 2 3
p53 pathway 4 4
Coagulation 4 2
0 2 4 6 8 10
−log10 P value
C
mTOR-dependent DEGs
EtOH
R1881
shmTOR
EV WT
↑922
↓1,391
↑1,333
↓1,526
−2.0 0 2.0
Z-score
(log2 FPKM+1)
+/− R1881
2,108
1,704
Up
Down
D
+/− R1881
p-HOXB13
(354)
mTOR
(3812)
↑39
↓67
% HOXB13-regulated genes
DEGs
p-HOXB13 & mTOR
p-HOXB13 only
+/− R1881
E
KLK2
STEAP4
HMGCS2
ACSL3
Relative mRNA expression
Vehicle
R1881
EV
HOXB13 WT
HOXB13 3A
HOXB13 3D
shHOXB13
F
KLK2
STEAP4
HMGCS2
ACSL3
Relative mRNA expression
Vehicle
R1881
EV
mTOR
shmTOR
G
KLK2
STEAP4
HMGCS2
ACSL3
Relative mRNA expression
Vehicle
R1881
DMSO
Torin1
Rapamycin

when mTOR was IP'd from extracts of Hela cells previously treated with insulin, an effect abolished by adding Torin1 directly to the reaction (**Fig. 3A**). MS analysis of the detected phospho-HOXB13 band from the mTOR kinase assay identified two prominent HOXB13 phosphorylation sites, threonine 8 and 41 (**Fig. 3B**). Mutations of these sites to alanine residues, individually or together, led to a partial reduction in HOXB13 phosphorylation by mTOR in the *in vitro* kinase assay (**Fig. 3C**). Although with a lower confidence score, serine 31 was also identified as a candidate HOXB13 phosphorylation site by MS, suggesting that mTOR phosphorylation at the primary sites, threonine 8 and 41, could induce subsequent phosphorylation at nearby sites. To test this hypothesis, we first mutated threonine 8 and 41 to aspartic acid residues to introduce phosphomimic sites in HOXB13. Interestingly, expression of the HOXB13 phosphomimic mutants T8D, T41D, and T8D+T41D in LNCaP cells resulted in the detection of an additional upper protein band, revealed to be the result of another phosphorylation event as the novel upper band vanished upon treatment with lambda phosphatase (**Fig. 3D** and **E**). Aside from the potential HOXB13 S31 phosphorylation site detected by MS, there are possible prospective false-negative phosphosites including S35, S250, and S254 that also warrant consideration. We thus changed these potential phosphorylated residues to alanine within the HOXB13 T8D+T41D phosphomimic mutant. Mutating serine residues at positions 250 and 254 to alanine did not eliminate the upper band (**Fig. 3F**). In stark contrast, mutating the HOXB13 phosphomimic T8D+T41D mutant at positions 31 and 35 from serine to alanine resulted in the complete disappearance of the upper band, implying that either S31 or S35 is the additional phosphorylation site(s) (**Fig. 3F**). HOXB13 T8D+T41D mutants harboring individual mutation of serine 31 or 35, confirmed that phosphorylation of S31 is responsible for the appearance of the additional upper band (**Fig. 3G**), thus supporting the MS data (**Fig. 3B**). Similar results were observed when the serine 31 to alanine mutation was introduced independently in the HOXB13 T8D or T4D mutant (Supplementary Fig. S2A). Importantly, the additional phosphorylation at serine 31 primed by phosphorylation at threonine residues 8 or 41 was not abolished by single alanine mutations at these sites, implying that phosphorylation of either T8 or T41 could trigger phosphorylation at S31 (**Fig. 3H**). No additional upper phosphorylation band was observed in a triple alanine mutant ($HOXB13^{3A}$) of the three phosphorylation sites T8, T41, and S31 (**Fig. 3I**). Notably, the additional phosphorylation of S31 was still found to be dependent on mTOR, as pharmacologic inhibition or genetic knockdown of mTOR inhibited the appearance of the upper band sparked by the HOXB13 phosphomimic mutants (Supplementary Fig. S2B and C). Further analysis showed that knockdown of RAPTOR, but not RICTOR, could reduce HOXB13 S31 phosphorylation (Supplementary Fig. S2D and S2E). A simplified model of HOXB13 phosphorylation by mTOR is illustrated in **Fig. 3J**.

HOXB13 phosphorylation promotes its degradation by SKP2

We next tested whether HOXB13 phosphorylation at the mTOR-targeted sites affects its protein stability. As shown by a cycloheximide chase assay in 293T cells, the triple phosphomimic mutant $HOXB13^{3D}$ (T8D, T41D, and S31D) degraded at a faster pace than both WT HOXB13 and $HOXB13^{3A}$ (**Fig. 4A**). Consistently, $HOXB13^{3D}$ showed markedly enhanced polyubiquitination compared with WT HOXB13 and $HOXB13^{3A}$, indicating its increased recognition by the proteasome for degradation (**Fig. 4B**). To identify potential E3 ligase(s) targeting HOXB13 for degradation, we used the ubiquitin ligase-substrate interaction tool $Ubibroswer^{1.0}$ (http://ubibrowser.bio-it.cn/ubibrowser). We focused our attention on the 3rd top ranked candidate E3 ligase SKP2 (Supplementary Fig. S3A) considering a recent proteomics study that identified the SKP2 family member SKP1 as a potential HOXB13 interactor (33). SKP2, also referred to as FBXL1, is a member of the F-box E3 ligase family which usually forms a SCF complex with SKP1/Cullin1 to trigger substrate ubiquitination and subsequent degradation in a phosphorylation-dependent manner (34–37). Co-IP experiments confirmed that both exogenously expressed HOXB13 in 293T cells and endogenous HOXB13 in LNCaP and PC3 cells interact with SKP2 (**Fig. 4C** and **D**; Supplementary Fig. S3B). Overexpression of SKP2 promoted HOXB13 polyubiquitination and destabilization (**Fig. 4E**; Supplementary Fig. S3C–S3E), while both genetic and pharmacologic inhibition of SKP2 stabilized HOXB13 protein levels in LNCaP and PC3 cells (**Fig. 4F**; Supplementary Fig. S3F and S3G). In further support that mTOR control of HOXB13 stability is SKP2-dependent, both genetic knockdown and pharmacologic inhibition of mTOR in LNCaP cells impaired HOXB13-SKP2 interaction (**Fig. 4G** and **H**), and $HOXB13^{3D}$ interacted more strongly with SKP2 compared with WT HOXB13 and $HOXB13^{3A}$ in 293T cells (**Fig. 4I**). Crucially, SKP2-induced HOXB13 degradation was abolished upon co-treatment with Torin1 in LNCaP cells (**Fig. 4J**), underscoring the necessity of mTOR-mediated HOXB13 phosphorylation for SKP2-mediated HOXB13 degradation (**Fig. 4K**).

HOXB13 phosphorylation specifies the HOXB13-dependent transcriptome

HOXB13, an important co-regulator of AR, is well-known to play a critical role in the control of gene expression. To establish whether HOXB13 phosphorylation at T8/T41/S31 affects its transcriptional

Figure 5.

HOXB13 phosphorylation governs its transcriptional function. **A,** Heat maps showing 354 DEGs ($P < 0.05$; $|Log_2FC| > 0.5$) found specifically altered by HOXB13 WT rescue compared with EV in HOXB13-depleted LNCaP cells whose levels also contrasted significantly compared with rescue with the phospho-deficient HOXB13 3A mutant under vehicle (EtOH) and/or R1881 24 hours conditions. Heat maps represent z-scaled $log_2(FPKM+1)$ values. Pie chart showing the subset of up- (200) and downregulated (154) DEGs dependent on phospho-HOXB13. **B,** Significantly enriched MSigDB Hallmark terms ($P < 0.05$) among the 354 DEGs identified in (**A**) with the number of associated up- and downregulated genes indicated. **C,** Heat maps showing 3812 DEGs ($P < 0.05$; $|Log_2FC| > 0.5$) significantly altered by mTOR rescue relative to EV in mTOR-depleted LNCaP cells under vehicle (EtOH) and/or R1881 24 hours conditions. Heat maps represent z-scaled $log_2(FPKM+1)$ values. Pie chart showing the subset of up- (2108) and downregulated (1704) mTOR-dependent DEGs. **D,** Cross-examination of phospho-HOXB13- (**A**) and mTOR-dependent (**C**) gene signatures ± R1881 revealed a set of 106 commonly regulated genes, representing ∼30% of phospho-HOXB13–dependent DEGs. **E,** RT-qPCR analysis of phospho-HOXB13 and mTOR co-regulated genes in LNCaP cells with HOXB13 knockdown rescued with HOXB13 WT or mutants ± R1881 (10 nmol/L, 24 hours). Statistical significance was calculated by comparing HOXB13 mutants to EV in vehicle (EtOH) or R1881 conditions. **F,** RT-qPCR analysis of phospho-HOXB13 and mTOR co-regulated genes in LNCaP cells with mTOR knockdown rescued with mTOR ± R1881 (10 nmol/L, 24 hours). Statistical significance was calculated by comparing mTOR rescue to EV in vehicle (EtOH) or R1881 conditions. **G,** RT-qPCR examination of LNCaP cells treated with mTOR inhibitor Torin1 (100 nmol/L) or Rapamycin (40 nmol/L) for 24 hours on the expression of phospho-HOXB13 and mTOR co-regulated genes. Statistical significance was calculated by comparing Torin1/Rapamycin- with DMSO-treated cells in either vehicle (EtOH) or R1881 conditions. Data in **E–G** represent means ± SEM of four independent experiments. Statistics were calculated by one-way ANOVA. *, $P < 0.05$; **, $P < 0.01$; ns, not significant.

activity, we conducted RNA-seq analyses of inducible LNCaP cell lines in which endogenous HOXB13 was depleted by shRNA-mediated knockdown and rescued by exogenous expression of WT HOXB13 or the HOXB13^{3A} mutant with YFP as the empty vector (EV) control in cells exposed to either vehicle (EtOH) or R1881 for 24 hours to stimulate the AR/mTOR signaling axis (Supplementary Table S1). Our analysis revealed a phospho-HOXB13–dependent gene signature ± R1881 comprised of 200 upregulated and 154 downregulated DEGs ($P < 0.05$, $|\text{Log}_2\text{FC}| > 0.5$) which were significantly and specifically driven by WT HOXB13 reexpression compared with EV control but also significantly reversed by the phospho-deficient HOXB13^{3A} mutant relative to WT HOXB13 (**Fig. 5A**; Supplementary Table S1). Notably, 72% of the 354 gene signature was established from R1881-treated cells, a condition leading to the simultaneous enhancement of both AR and mTOR activity, upstream regulators of HOXB13 protein destabilization found herein to involve mTOR-mediated phosphorylation. Functional interrogation of the 354-gene set uncovered several important enriched MSigDB Hallmark terms including downregulation of the androgen response signature and bi-directional regulation of TNFα/NF-κB signaling (**Fig. 5B**). RT-qPCR confirmed that both HOXB13 and the phospho-mimic HOXB13^{3D} mutant but not HOXB13^{3A} could repress androgen-mediated upregulation of the IκBα-encoding gene *NFKBIA*, a key inhibitor of NF-κB transcriptional activity (Supplementary Fig. S4A). Reversely, pharmacologic inhibition of mTOR by Torin1 or Rapamycin promoted *NFKBIA* expression (Supplementary Fig. S4B), supporting mTOR as an upstream kinase directing phospho-HOXB13–mediated regulation of NF-κB signaling. Consistently, HOXB13 fostered the nuclear translocation and activation of NF-κB (p65 and p50) in a phospho-dependent manner by releasing the inhibitory effect of NFKBIA (Supplementary Fig. S4C).

To reinforce the molecular link between phospho-HOXB13 T8/T41/S31 and mTOR kinase, we established inducible shRNA-mediated mTOR knockdown LNCaP cell lines rescued with mTOR or YFP as control (Supplementary Fig. S4D) and used these cell lines to monitor functional overlap between phospho-HOXB13– and mTOR-driven gene signatures. mTOR activation led to a robust upregulation of 1704 genes and downregulation of 2108 genes ($P < 0.05$; $|\text{Log}_2\text{FC}| > 0.5$) in cells exposed to either vehicle (EtOH) or R1881 for 24 hours (**Fig. 5C**; Supplementary Table S2). Importantly, 30% of the phospho-HOXB13–driven genes (106 of 354) were also regulated by mTOR in a consistent manner ± R1881 (**Fig. 5D**; Supplementary Fig. S4E; and Supplementary Table S2). The majority of the 106 shared cotargets were downregulated by p-HOXB13 and mTOR of which several were validated by RT-qPCR including androgen response genes *KLK2* and *STEAP4* and lipid metabolic genes *HMGCS2* and *ACSL3* (**Fig. 5E** and **F**). The repressive action of HOXB13 on the examined genes were mimicked by the HOXB13^{3D} mutant but lost by the HOXB13^{3A} mutant, indicating a dominant effect of HOXB13 phosphorylation on their transcriptional control (**Fig. 5E**). In contrast to the response observed by mTOR activation, inhibition of mTOR by Torin1 or Rapamycin de-repressed the expression of these genes (**Fig. 5G**).

HOXB13 phosphorylation promotes its oncogenic function

To investigate the impact of HOXB13 phosphorylation on prostate cancer cell growth and tumorigenesis, we exploited our established genetically engineered LNCaP cell lines with stable knockdown of endogenous HOXB13 rescued by the inducible expression of WT HOXB13, HOXB13^{3A}, and HOXB13^{3D} (**Fig. 6A**). In addition, cells reexpressing HOXB13^{G84E} harboring a G84E mutation, a variant associated with increased prostate cancer risk (10), were used as a control for comparison (**Fig. 6A**). Cell colony formation assay showed a decreased LNCaP cell growth rate upon HOXB13 depletion, found rescued and even enhanced by reintroduction of HOXB13^{3D} and HOXB13^{G84E} phosphomimic mutants but not the phospho-deficient HOXB13^{3A} mutant (**Fig. 6B**). Similarly, HOXB13^{3D} and HOXB13^{G84E} mutants promoted HOXB13-depleted LNCaP cell proliferation unlike the HOXB13^{3A} mutant (Supplementary Fig. S5A). To further support the *in vitro* findings, the distinct LNCaP clones were inoculated subcutaneously in NSG-nude mice and xenograft tumor development was monitored to evaluate the oncogenic potential of the HOXB13 mutants in an *in vivo* model system. The tumor incidence was 100% (6/6) for all xenograft models. Critically, in stark contrast to HOXB13^{3A}, WT HOXB13 and HOXB13^{3D} phosphomimic mutant significantly enhanced xenograft tumorigenicity compared with the HOXB13 knockdown model (**Fig. 6C** and **D**), thus recapitulating the phenotypes observed *in vitro*. Although LNCaP cells expressing the HOXB13^{G84E} mutant displayed enhanced cellular growth and proliferation *in vitro*, its impact on tumor growth *in vivo* was not significant (**Fig. 6C** and **D**). This observation is consistent with previous reports demonstrating that HOXB13^{G84E} confers a greater prostate cancer risk without obvious phenotypic changes (38). Examination of xenograft tumors confirmed both the exogenous expression of WT HOXB13 and HOXB13 mutants and that WT HOXB13 and HOXB13^{3D} but not phospho-deficient HOXB13^{3A} can downregulate *KLK2*, *STEAP4*, *HMGCS2*, and *ACSL3* transcription (Supplementary Fig. S5B and S5C), genes validated in **Fig. 5** to be co-regulated by both phospho-HOXB13 and mTOR. Notably, HOXB13^{G84E} was found to repress the expression of 3 of 4 of these genes in xenograft tumors, signifying that the increased tumorigenicity observed by HOXB13^{3D} involves dysregulation of other genes.

Together, the data demonstrate that phosphorylation of T8, T41, and S31 on HOXB13 promotes its oncogenic activation. Due to the lack of commercially available antibodies and difficulty in generating those specifically targeting each identified HOXB13 phosphorylated residue, we evaluated the clinical relevance of the identified phospho-HOXB13 354-gene signature on prostate cancer progression and aggressiveness in human clinical specimens. First, we performed unsupervised hierarchical clustering analysis on patient samples from the Tomlins and colleagues cohort (ref. 31; GSE6099) resulting in a strong discrimination (90%) between normal and epithelial benign cells, localized prostate cancer, and hormone-refractory (CRPC) metastatic prostate cancer based on 127 of 354 mapped genes with available expression data (**Fig. 6E**; Supplementary Table S1). Next, using this validated phospho-HOXB13–driven 127-gene subset, we were also able to robustly distinguish normal benign prostate tissue, localized primary prostate cancer and metastatic prostate cancer tissue in two independent cohorts, GSE3325 (32) and GSE8511 (**Fig. 6E**), reinforcing the relationship between oncogenic phospho-HOXB13 action and prostate cancer progression.

Discussion

HOXB13 is known to exert both oncogenic and tumor suppressive roles in prostate cancer development through its interaction with AR, MEIS1 and the HDAC3-NCoR/SMART complex (6, 33, 39). In recent work, we found strong evidence supporting genomic interaction between chromatin-bound mTOR and HOXB13 in several prostate cancer cell lines (24, 26) whereas mTOR was also identified as a potential regulatory cofactor of HOXB13 in LNCaP cells (33). However, how these interactions affect the activity of each component of this complex and, more importantly, how a potential mTOR–HOXB13

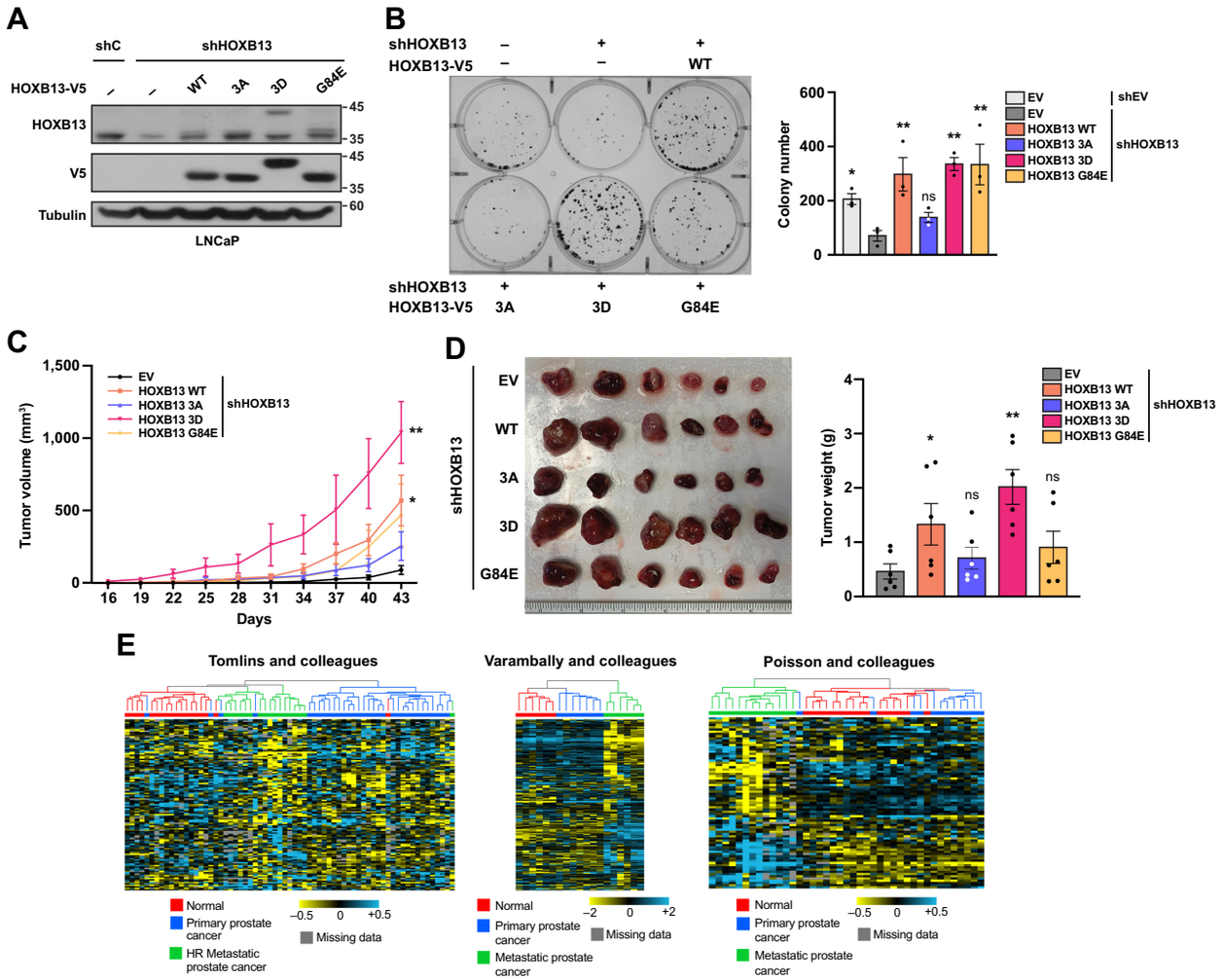

Figure 6.

HOXB13 phosphorylation promotes its oncogenic function. **A,** LNCaP cells with HOXB13 knockdown were rescued by either EV, WT-HOXB13, 3A-HOXB13, 3D-HOXB13, or G84E-HOXB13. Both knockdown and overexpression were simultaneously induced by 1 μg/mL Doxycycline for 3 days. **B,** Colony formation assay was performed using stable LNCaP cells in (A) for ∼3 weeks. Colony number was counted using Image J software. Data represent means ± SEM of three independent experiments. Statistics were calculated using shHOXB13+EV-treated cells as the reference. **C,** Xenograft tumor growth assay was performed using LNCaP cells with HOXB13 knockdown rescued with either WT HOXB13 or different HOXB13 mutants. Immuno-deficient NSG mice were given 2 mg/mL Doxycycline water. Statistics were calculated by comparing HOXB13 mutants with EV at day 43 from six biological replicates per group. **D,** Image and quantification of end-point xenograft tumors from (**C**). **E,** Unsupervised hierarchical clustering analysis with the 354 phospho-HOXB13–dependent gene signature as defined in **Fig. 5A** was first tested on the Tomlins and colleagues (31) cohort (GSE6099), resulting in 127 mapped genes capable of discriminating between normal or peri-tumoral epithelial cells (Normal), localized primary prostate cancer tissues (Primary prostate cancer), and hormone-refractory metastatic prostate cancer (HR Metastatic prostate cancer). The validated 127 gene subset was subsequently used on two independent clinical cohorts Varambally and colleagues (GSE3325) and Poisson and colleagues (GSE8511) also capable of distinguishing between normal benign prostate tissues, localized primary prostate cancer tissues and metastatic prostate cancer tissues. Data in **B–D** represent means ± SEM. Statistics were calculated by one-way ANOVA. *, $P < 0.05$; **, $P < 0.01$; ns, not significant.

axis transcriptional axis could influence prostate cancer progression remained to be investigated. Herein, we report that mTOR and HOXB13 directly interact with each other and that mTOR-mediated phosphorylation of HOXB13 activates its oncogenic function in prostate cancer cells.

Mechanistically, we uncovered that the mTOR–HOXB13 interaction involves the carboxy-terminal region of mTOR harboring the kinase domain and the amino-terminal region encoding the MEIS domain of HOXB13. Our work elucidated that this interaction leads to the phosphorylation by mTOR of three residues within the amino-terminal domain of HOXB13, whereby phosphorylation of T8/T41 primes its subsequent phosphorylation at S31. Serine 31 of HOXB13 is followed by a proline residue and mTOR is known to phosphorylate its substrates in a proline-directed manner (19, 40). Although S31 phosphorylation was found sensitive to mTOR inhibition, it is also plausible that other kinases contribute to the phosphorylation of these residues. Along these lines, CDK1 and CDK9 were identified as possible HOXB13 interactors in a recent HOXB13 interactome study (33) and CDKs are proline-directed kinases. In addition, the sequences surrounding HOXB13 S31 and S35 also predict recognition by GSK3α/β given their kinase consensus motif, Ser/Thr-x-x-x-Ser/Thr. However, our results indicate that GSK3α/β

is not the second kinase implicated in HOXB13 S31 phosphorylation as GSK3α/β would first require phosphorylation at S35 to phosphorylate S31 and our results showed that the S35A mutation did not abolish the upper band (S31 phosphorylation) of HOXB13 (**Fig. 3G**). In effect, mTOR-mediated phosphorylation of HOXB13 is better aligned with 4EBP1 phosphorylation by mTOR, whereby T37/T46 phosphorylation primes its further phosphorylation at T70/S65 with the second kinase proposed to be mTOR or another proline-directed kinase like ERK2 (41–43). Phosphorylation of HOXB13 at T8/T41/S31 was found to increase its association with E3 ligase SKP2, thus triggering its polyubiquitination and subsequent degradation. Proteosome-mediated turnover of transcription factors has been shown to contribute significantly to transcriptional activation (44, 45), and may thus constitute an important mechanism by which HOXB13 activity is controlled in both normal and transformed cells. Indeed, SKP2 has been shown to act as a coactivator of the oncoprotein Myc uniting its transcriptional activity and degradation (46, 47). It will also be of great interest to identify potential phosphatase(s) for HOXB13 that may equally participate in the regulation of HOXB13 protein stability as well as the possible involvement of other E3 ligases and deubiquitinases in this process. In agreement with this notion, the phosphatase calcineurin was recently shown to dephosphorylate HOXB13 at S204 (16).

RNA-seq profiling revealed that genes associated with the androgen response, TNFα/NF-κB signaling, and lipid metabolism were among molecular signatures found modulated among the 354-geneset found regulated by HOXB13 phosphorylation. While HOXB13 has previously been shown to promote prostate cancer metastasis through upregulation of NF-κB signaling via *NFKBIA* downregulation (12) as well as act as a key modulator of the androgen response (6), our findings emphasize the importance of mTOR-mediated phosphorylation of HOXB13 in dictating the prostate cancer transcriptome, undoubtedly altering prostate cancer oncogenesis. Nearly one third of the phospho-HOXB13–dependent gene signature was similarly regulated by mTOR, thus reinforcing the functional link of mTOR signaling acting upstream of HOXB13. Ultimately, the profound transcriptional reprogramming driven by phospho-competent HOXB13 resulted in an acceleration of LNCaP cellular growth and proliferation *in vitro* as well as LNCaP xenograft tumor growth *in vivo*. Notably, the $HOXB13^{3D}$ phosphomimic mutant (T8D/T41D/S31D) displayed greater xenograft tumorigenesis compared with the phosphomimicking mutant $HOXB13^{G84E}$, although the precise underlying oncogenic mechanisms require further study. It is conceivable that phosphorylation of HOXB13 at T8/T41/S31 influences its interactome on the chromatin and distinct AR/HOXB13 protein complexes combined with other cofactors could be responsible for the differential transcriptional effects observed. HDAC3 was recently found to interact specifically with HOXB13 but not $HOXB13^{G84E}$, in an AR-independent manner, underlying the ability of HOXB13 to suppress *de novo* lipogenesis and inhibit prostate cancer metastasis (33).

mTOR kinase is a homeostatic sensor that plays a major role in the control of cell growth (19), and dysregulation of the canonical mTOR pathway and its nuclear activity have been linked to prostate cancer aggressiveness and poor outcome (24, 48–50). Here we identified a critical link between mTOR activation, HOXB13 phosphorylation and prostate cancer cell growth. Significantly, we showed that expression of a HOXB13 triple phosphomimetic mutant involving identified mTOR-targeted residues, but not the non-phosphorylatable mutant, promotes prostate cancer cellular growth *in vitro* and tumor growth *in vivo* in a xenograft model system. In addition, we established that a functional phospho-HOXB13–dependent gene signature can robustly differentiate normal prostate tissues, primary prostate cancer, and metastatic prostate cancer in three independent human clinical cohorts emphasizing the importance of the previously unrecognized mTOR/HOXB13 regulatory axis during prostate cancer development. While activation of canonical mTOR signaling takes place in the cytoplasm, recent work clearly demonstrated that mTOR and HOXB13 associate on chromatin in prostate cancer cells (26), confirmed herein to interact together in the nucleus of LNCaP cells, indicating that mTOR phosphorylation of HOXB13 likely occurs in the nucleus. Taken together, this work exposed a previously unrecognized mTOR-dependent phosphorylation cascade dictating HOXB13 oncogenic activity in prostate cancer.

Authors' Disclosures

Y. Chen reports grants from Canadian Institutes of Health Research (CIHR); and grants from Terry Fox Foundation during the conduct of the study. C.R. Dufour reports grants from CIHR, Terry Fox Research Institute Team; and grants from Cancer Research Society and Génome Québec during the conduct of the study. L. Han reports grants from CIHR, Terry Fox Research Institute; and grants from Cancer Research Society during the conduct of the study. T. Li reports grants from CIHR, Terry Fox Research Institute Team; and grants from Cancer Research Society and Génome Québec during the conduct of the study. H. Xia reports grants from CIHR, Terry Fox Research Institute; and grants from Cancer Research Society during the conduct of the study. V. Giguere reports grants from CIHR, Terry Fox Research Institute; and grants from Cancer Research Society during the conduct of the study.

Authors' Contributions

Y. Chen: Conceptualization, data curation, formal analysis, methodology, writing–original draft. **C.R. Dufour:** Conceptualization, data curation, formal analysis, project administration, writing–review and editing. **L. Han:** Data curation. **T. Li:** Data curation. **H. Xia:** Data curation. **V. Giguere:** Conceptualization, supervision, funding acquisition, writing–original draft, writing–review and editing.

Acknowledgments

We thank members of the Giguère's laboratory for daily assistance and helpful discussions; Dr. D. Faubert and his team at the Institut de Recherches Cliniques de Montréal for Mass Spectrometry analysis; Drs. M. Tremblay and J. Teodoro (McGill University) for advice on the project; and Dr. E. Audet-Walsh (Laval University) for suggestions on clinical correlation analysis. This work was supported by a Foundation grant from the CIHR to V.G. (FDT-156254), a Terry Fox Research Institute Team grant (PPG-1091), and a co-funded operating grant from the Cancer Research Society and Génome Québec (CRS-25085). L. Han is supported by a Canderel and Fond de recherches du Québec – Santé (FRQS) studentship. X. Hui was a recipient of a FRQS studentship.

The publication costs of this article were defrayed in part by the payment of publication fees. Therefore, and solely to indicate this fact, this article is hereby marked "advertisement" in accordance with 18 USC section 1734.

Note

Supplementary data for this article are available at Molecular Cancer Research Online (http://mcr.aacrjournals.org/).

Received February 9, 2023; revised May 23, 2023; accepted June 27, 2023; published first July 6, 2023.

References

1. Harris WP, Mostaghel EA, Nelson PS, Montgomery B. Androgen deprivation therapy: progress in understanding mechanisms of resistance and optimizing androgen depletion. Nat Clin Pract Urol 2009;6:76–85.
2. Pomerantz MM, Li F, Takeda DY, Lenci R, Chonkar A, Chabot M, et al. The androgen receptor cistrome is extensively reprogrammed in human prostate tumorigenesis. Nat Genet 2015;47:1346–51.
3. Ku SY, Gleave ME, Beltran H. Towards precision oncology in advanced prostate cancer. Nat Rev Urol 2019;16:645–54.
4. Giguère V. DNA-PK, nuclear mTOR, and the androgen pathway in prostate cancer. Trends Cancer 2020;6:337–47.
5. Economides KD, Capecchi MR. Hoxb13 is required for normal differentiation and secretory function of the ventral prostate. Development 2003;130: 2061–9.
6. Norris JD, Chang CY, Wittmann BM, Kunder RS, Cui H, Fan D, et al. The homeodomain protein HOXB13 regulates the cellular response to androgens. Mol Cell 2009;36:405–16.
7. Chen Z, Wu D, Thomas-Ahner JM, Lu C, Zhao P, Zhang Q, et al. Diverse AR-V7 cistromes in castration-resistant prostate cancer are governed by HoxB13. Proc Natl Acad Sci USA 2018;115:6810–5.
8. Huang Q, Whitington T, Gao P, Lindberg JF, Yang Y, Sun J, et al. A prostate cancer susceptibility allele at 6q22 increases RFX6 expression by modulating HOXB13 chromatin binding. Nat Genet 2014;46:126–35.
9. Yao J, Chen Y, Nguyen DT, Thompson ZJ, Eroshkin AM, Nerlakanti N, et al. The homeobox gene, HOXB13, regulates a mitotic protein-kinase interaction network in metastatic prostate cancers. Sci Rep 2019;9:9715.
10. Ewing CM, Ray AM, Lange EM, Zuhlke KA, Robbins CM, Tembe WD, et al. Germline mutations in HOXB13 and prostate-cancer risk. N Engl J Med 2012; 366:141–9.
11. Kim YR, Oh KJ, Park RY, Xuan NT, Kang TW, Kwon DD, et al. HOXB13 promotes androgen independent growth of LNCaP prostate cancer cells by the activation of E2F signaling. Mol Cancer 2010;9:124.
12. Kim YR, Kim IJ, Kang TW, Choi C, Kim KK, Kim MS, et al. HOXB13 downregulates intracellular zinc and increases NF-κB signaling to promote prostate cancer metastasis. Oncogene 2014;33:4558–67.
13. Jung C, Kim RS, Lee SJ, Wang C, Jeng MH. HOXB13 homeodomain protein suppresses the growth of prostate cancer cells by the negative regulation of T-cell factor 4. Cancer Res 2004;64:3046–51.
14. Jung C, Kim RS, Zhang HJ, Lee SJ, Jeng MH. HOXB13 induces growth suppression of prostate cancer cells as a repressor of hormone-activated androgen receptor signaling. Cancer Res 2004;64:9185–92.
15. Liu B, Wang T, Wang H, Zhang L, Xu F, Fang R, et al. Oncoprotein HBXIP enhances HOXB13 acetylation and co-activates HOXB13 to confer tamoxifen resistance in breast cancer. J Hematol Oncol 2018;11:26.
16. Nguyen NUN, Canseco DC, Xiao F, Nakada Y, Li S, Lam NT, et al. A calcineurin–Hoxb13 axis regulates growth mode of mammalian cardiomyocytes. Nature 2020;582:271–6.
17. Imseng S, Aylett CH, Maier T. Architecture and activation of phosphatidylinositol 3-kinase related kinases. Curr Opin Struct Biol 2018;49:177–89.
18. Blenis J. TOR, the Gateway to cellular metabolism, cell growth, and disease. Cell 2017;171:10–3.
19. Battaglioni S, Benjamin D, Walchli M, Maier T, Hall MN. mTOR substrate phosphorylation in growth control. Cell 2022;185:1814–36.
20. Kim J, Guan KL. mTOR as a central hub of nutrient signalling and cell growth. Nat Cell Biol 2019;21:63–71.
21. Wan W, You Z, Xu Y, Zhou L, Guan Z, Peng C, et al. mTORC1 phosphorylates acetyltransferase p300 to regulate autophagy and lipogenesis. Mol Cell 2017;68: 323–35.
22. Giguère V. Canonical signaling and nuclear activity of mTOR: a teamwork effort to regulate metabolism and cell growth. Febs J 2018;285:1572–88.
23. Laribee RN, Weisman R. Nuclear functions of TOR: impact on transcription and the epigenome. Genes 2020;11:641.
24. Audet-Walsh E, Dufour CR, Yee T, Zouanat FZ, Yan M, Kalloghlian G, et al. Nuclear mTOR acts as a transcriptional integrator of the androgen signaling pathway in prostate cancer. Genes Dev 2017;31:1228–42.
25. Audet-Walsh E, Vernier M, Yee T, Laflamme C, Li S, Chen Y, et al. SREBF1 activity Is regulated by an AR/mTOR nuclear axis in prostate cancer. Mol Cancer Res 2018;16:1396–405.
26. Dufour CR, Scholtes C, Yan M, Chen Y, Han L, Li T, et al. The mTOR chromatin-bound interactome in prostate cancer. Cell Rep 2022;38:110534.
27. Xu Y, Chen SY, Ross KN, Balk SP. Androgens induce prostate cancer cell proliferation through mammalian target of rapamycin activation and posttranscriptional increases in cyclin D proteins. Cancer Res 2006;66:7783–92.
28. Massie CE, Lynch A, Ramos-Montoya A, Boren J, Stark R, Fazli L, et al. The androgen receptor fuels prostate cancer by regulating central metabolism and biosynthesis. EMBO J 2011;30:2719–33.
29. Chen EY, Tan CM, Kou Y, Duan Q, Wang Z, Meirelles GV, et al. Enrichr: interactive and collaborative HTML5 gene list enrichment analysis tool. BMC Bioinf 2013;14:128.
30. de Hoon MJ, Imoto S, Nolan J, Miyano S. Open source clustering software. Bioinformatics 2004;20:1453–4.
31. Tomlins SA, Laxman B, Dhanasekaran SM, Helgeson BE, Cao X, Morris DS, et al. Distinct classes of chromosomal rearrangements create oncogenic ETS gene fusions in prostate cancer. Nature 2007;448:595–9.
32. Varambally S, Yu J, Laxman B, Rhodes DR, Mehra R, Tomlins SA, et al. Integrative genomic and proteomic analysis of prostate cancer reveals signatures of metastatic progression. Cancer Cell 2005;8:393–406.
33. Lu X, Fong KW, Gritsina G, Wang F, Baca SC, Brea LT, et al. HOXB13 suppresses de novo lipogenesis through HDAC3-mediated epigenetic reprogramming in prostate cancer. Nat Genet 2022;54:670–83.
34. Carrano AC, Eytan E, Hershko A, Pagano M. SKP2 is required for ubiquitin-mediated degradation of the CDK inhibitor p27. Nat Cell Biol 1999;1:193–9.
35. Chan CH, Li CF, Yang WL, Gao Y, Lee SW, Feng Z, et al. The Skp2-SCF E3 ligase regulates Akt ubiquitination, glycolysis, herceptin sensitivity, and tumorigenesis. Cell 2012;149:1098–111.
36. Yumimoto K, Yamauchi Y, Nakayama KI. F-Box proteins and cancer. Cancers 2020;12.
37. Hunter T. The age of crosstalk: phosphorylation, ubiquitination, and beyond. Mol Cell 2007;28:730–8.
38. Cardoso M, Maia S, Paulo P, Teixeira MR. Oncogenic mechanisms of HOXB13 missense mutations in prostate carcinogenesis. Oncoscience 2016;3:288–96.
39. VanOpstall C, Perike S, Brechka H, Gillard M, Lamperis S, Zhu B, et al. MEIS-mediated suppression of human prostate cancer growth and metastasis through HOXB13-dependent regulation of proteoglycans. Elife 2020;9:e53600.
40. Hsu PP, Kang SA, Rameseder J, Zhang Y, Ottina KA, Lim D, et al. The mTOR-regulated phosphoproteome reveals a mechanism of mTORC1-mediated inhibition of growth factor signaling. Science 2011;332:1317–22.
41. Gingras AC, Raught B, Gygi SP, Niedzwiecka A, Miron M, Burley SK, et al. Hierarchical phosphorylation of the translation inhibitor 4E-BP1. Genes Dev 2001;15:2852–64.
42. Gingras AC, Gygi SP, Raught B, Polakiewicz RD, Abraham RT, Hoekstra MF, et al. Regulation of 4E-BP1 phosphorylation: a novel two-step mechanism. Genes Dev 1999;13:1422–37.
43. Qin X, Jiang B, Zhang Y. 4E-BP1, a multifactor regulated multifunctional protein. Cell Cycle 2016;15:781–6.
44. Lonard DM, Nawaz Z, Smith CL, O'Malley BW. The 26S proteasome is required for estrogen receptor-alpha and coactivator turnover and for efficient estrogen receptor-alpha transactivation. Mol Cell 2000;5:939–48.
45. Wang X, Arceci A, Bird K, Mills CA, Choudhury R, Kernan JL, et al. VprBP/DCAF1 regulates the degradation and nonproteolytic activation of the cell cycle transcription factor FoxM1. Mol Cell Biol 2017;37:e00609–16.
46. Kim SY, Herbst A, Tworkowski KA, Salghetti SE, Tansey WP. Skp2 regulates Myc protein stability and activity. Mol Cell 2003;11:1177–88.
47. von der Lehr N, Johansson S, Wu S, Bahram F, Castell A, Cetinkaya C, et al. The F-box protein Skp2 participates in c-Myc proteosomal degradation and acts as a cofactor for c-Myc-regulated transcription. Mol Cell 2003;11:1189–200.
48. Taylor BS, Schultz N, Hieronymus H, Gopalan A, Xiao Y, Carver BS, et al. Integrative genomic profiling of human prostate cancer. Cancer Cell 2010;18: 11–22.
49. Grasso CS, Wu YM, Robinson DR, Cao X, Dhanasekaran SM, Khan AP, et al. The mutational landscape of lethal castration-resistant prostate cancer. Nature 2012; 487:239–43.
50. Kumar A, Coleman I, Morrissey C, Zhang X, True LD, Gulati R, et al. Substantial interindividual and limited intraindividual genomic diversity among tumors from men with metastatic prostate cancer. Nat Med 2016;22:369–78.